The Effect of the 2013-2016 High Temperature Anomaly in the Subarctic Northeast Pacific (The "Blob") on Net Community Production

Bo Yang[1†], Steven R. Emerson[1], M. Angelica Peña[2]

[1] School of Oceanography, University of Washington, Seattle, WA 98195, USA

[2] Institute of Ocean Sciences, Fisheries and Oceans Canada, PO Box 6000, Sidney, BC, Canada, V8L 4B2

[†]Present Address: Department of Environmental Sciences, University of Virginia, Charlottesville, VA 22904

Corresponding author: Bo Yang (by3jr@virginia.edu)

Email address: Steven R. Emerson (emerson@uw.edu), M. Angelica Peña (Angelica.Pena@dfo-mpo.gc.ca)

Key words: The warm blob, net community production, Ocean Station Papa

Abstract

A large anomalously warm water patch (the "Blob") appeared in the NE Pacific Ocean in the winter of 2013–14 and persisted through 2016 causing strong positive upper ocean temperature anomalies at Ocean Station Papa (OSP, 50°N, 145°W). The effect of the temperature anomalies on annual net community production (ANCP) was determined by upper ocean chemical mass balances of O_2 and DIC using data from a profiling float and a surface mooring. Year-round oxygen mass balance in the upper ocean (0 to 91–111 m) indicates that ANCP decreased after the first year when warmer water invaded this area and then returned to the "pre-blob" value (2.4, 0.8, 2.1, and 1.6 mol C m^{-2} yr^{-1} from 2012 to 2016, with a mean value of 1.7 ± 0.7 mol C m^{-2} yr^{-1}). ANCP determined from DIC mass balance has a mean value that is similar within the errors as that from the O_2 mass balance but without significant trend (2.0, 2.1, 2.6, and 3.0 mol C m^{-2} yr^{-1} with a mean value of 2.4 ± 0.6 mol C m^{-2} yr^{-1}). This is likely due to differences in the air-sea gas exchange, which is a major term for both mass balances. Oxygen has a residence time with respect to gas exchange of about one month while the CO_2 gas exchange response time is more like a year. Therefore the biologically induced oxygen saturation anomaly responds fast enough to record annual changes whereas that for CO_2 does not. Phytoplankton pigment analysis from the upper ocean shows lower chlorophyll-*a* concentrations and changes in plankton community composition (greater relative abundance of picoplankton) in the year after the warm water patch entered the area than in previous and subsequent years. Our analysis of multiple physical and biological processes that may have caused the ANCP decrease after warm water entered the area suggests that it was most likely due to the temperature-induced changes in biological processes.

1 Introduction

Net community production (NCP) in the upper ocean is defined as net organic carbon production, which equals biological production minus respiration. At steady state when integrated over a period of at least one year, the annual NCP (ANCP) is equivalent to the flux of biologically-produced organic matter from the upper ocean to the interior. Both biological production and respiration processes are temperature dependent, and heterotrophic activities such as community respiration and zooplankton grazing are usually considered to be more sensitive to temperature change than autotrophic production (Allen et al., 2005; Brown et al., 2004; Gillooly et al., 2001; López-Urrutia et al., 2006; Regaudie-De-Gioux and Duarte, 2012; Rose and Caron, 2007). This implies that rising temperature should lead to enhanced heterotrophy and lower NCP (López-Urrutia et al., 2006). In contrast, it has also been suggested (e.g., Chen and Laws, 2017) that the main effect of temperature on community metabolism is likely due to differences in phytoplankton community composition (e.g. cyanobacteria dominate in warm, oligotrophic waters, whereas diatoms dominate in cold, nutrient-rich areas) rather than to lower temperature sensitivity of phytoplankton production.

From the winter of 2013, a large anomalously warm water patch (the "Blob") appeared in the NE Pacific Ocean (Bond et al., 2015). The "Blob" had stretched from Alaska to Baja California by the end of 2015 (Di Lorenzo and Mantua, 2016) and caused widespread changes in the marine ecosystem, such as geographical shifts of plankton species, harmful algal blooms, and strandings of fishes, marine mammals, and seabirds (Cavole et al., 2016; Peña et al., 2018). Here we calculate the ANCP with upper ocean oxygen (O_2) and dissolved inorganic carbon (DIC) mass balances using data from Ocean Station Papa in the NE Pacific (OSP, 50°N, 145°W, Figure 1), to determine if there were significant NCP changes during the anomalous warm event. The

monthly Sea Surface Temperature Anomaly (SSTA) at OSP from 2012 to 2016 (Figure 2) indicates that for most of the 1st year (starting from June 2012) sea surface temperature (SST) was lower than usual, but then transitioned to strong positive temperature anomaly from 2013 to 2014. The positive anomaly continued with a magnitude of ~ 2°C to June 2015, and then dropped back to "normal" in the summer of 2016.

Our field location is in the subarctic northeast Pacific Ocean at OSP, where repeat hydrographic cruises have been carried out since 1981 by Fisheries and Oceans Canada with a frequency of two to three times per year (Freeland, 2007). A NOAA surface mooring has been deployed at OSP since 2007, for physical and biogeochemical measurements such as temperature, salinity, wind, ocean current, radiation, oxygen and total gas pressure, pH, and carbon dioxide (CO_2) (Emerson et al., 2011; Cronin et al., 2015; Fassbender et al., 2016). In addition, Argo profiling floats have been deployed near OSP since the 2000s (Freeland and Cummins, 2005). The first floats measured only temperature, salinity, and pressure but then measurements of oxygen and nitrate were added (Bushinsky and Emerson, 2015; Johnson et al., 2009). NCP at OSP has been determined using various approaches over the years, including bottle incubations (Wong, 1995), ^{234}Th methods (Charette et al., 1999), carbon/nutrient drawdown (Fassbender et al., 2016; Plant et al., 2016; Takahashi et al., 1993; Wong et al., 2002a, 2002b), and oxygen mass balance (Bushinsky and Emerson, 2015; Emerson, 1987; Emerson et al., 1991, 1993; Giesbrecht et al., 2012; Juranek et al., 2012; Plant et al., 2016).

2 Methods

2.1 Measurements of O_2, DIC, and phytoplankton biomass

Autonomous in situ oxygen measurements were made on a profiling float deployed by the University of Washington (Special Oxygen Sensor Argo float, SOS-Argo F8397, WMO #

5903743, Figure 1). The complete dataset is available at https://sites.google.com/a/uw.edu/sosargo/, and some of the data have been published previously by Bushinsky and Emerson (2015) and Yang et al. (2017). Oxygen measurements on the SOS-Argo float were obtained using an Aanderaa optode oxygen sensor with air-calibration mechanism (Bushinsky et al., 2016) capable of providing the air-sea difference in oxygen concentration with an accuracy of about ± 0.2 % and a vertical resolution of 3-5 m in the top 200 m of water column. This float was operated at a cycle interval of ~ 5 days covering depths from surface to 1800 m.

Partial pressure of seawater CO_2 (pCO_2), temperature, and salinity data were obtained from the NOAA mooring at OSP (WMO # 4800400). The complete dataset is available at http://cdiac.ornl.gov/oceans/Moorings/Papa_145W_50N.html, and some of the data were published by Fassbender et al. (2016). DIC was calculated using the total alkalinity (TA)-pCO_2 pair in CO2sys program Version 1.1 (van Heuven et al., 2011), where TA was calculated using the linear relationship with salinity developed in Fassbender et al. (2016) ($TA = 37 \times S + 988$) for the OSP vicinity. The calculation was performed on the total pH scale using the carbonate dissociation constants (K_1' and K_2') of Lueker et al. (2000), the HSO_4^- dissociation constant from Dickson et al. (1990), and the B_T/S ratio from Lee et al. (2010). The DIC data were normalized to the annual mean salinity at OSP (32.5), to eliminate the influence from evaporation/dilution.

Water samples for phytoplankton abundance and community composition were collected at OSP during 14 Line P repeat hydrographic cruises aboard the CCGS John P. Tully from 2012 to 2016 (February, June, and August for each year). Phytoplankton biomass, measured as total chlorophyll *a* (chl-*a*) concentrations, and the contribution of the main taxonomic groups of phytoplankton to chl-*a* were determined from high performance liquid chromatography (HPLC)

105 measurements of phytoplankton pigment concentrations (chlorophylls and carotenoids, Zapata
106 et al. 2000) followed by CHEMTAX v1.95 analysis (Mackey et al., 1996). Eight algal groups
107 were included in the chemotaxonomic analysis: diatoms, haptophytes, chlorophytes,
108 pelagophytes, prasinophytes, dinoflagellates, cryptophytes, and cyanobacteria. However,
109 cryptophytes were not found since their biomarker pigment, alloxanthin was not detected in any
110 of our samples. Pigment ratios for each algal group were obtained from Higgins et al. (2011) and
111 used as 'seed' values for multiple trials (60 runs) from randomized starting points, as described
112 by Wright et al. (2009). The same initial pigment ratios (Table 1a) were used in all cruises but
113 each cruise was run separately to allow potential variations in the CHEMTAX optimization to be
114 expressed. The range of final pigment ratios are given in Table 1b and the final ratios for each
115 cruise are given in Peña et al. (2018). The six best solutions (those with the lowest residuals)
116 were averaged for estimating the taxonomic abundances.

117 **2.2 Models used for NCP calculation**

118 **2.2.1 Oxygen mass balance model**

119 Oxygen, temperature, and salinity data from SOS-Argo F8397 and wind speed (U_{10}) data
120 from NOAA PMEL OSP mooring (https://www.pmel.noaa.gov/ocs/data/disdel/,
121 https://www.pmel.noaa.gov/ocs/data/fluxdisdel/) were used in a multi-layer upper ocean O_2
122 mass balance model to calculate NCP. This model frame (Figure 3) is similar to what was used
123 in Bushinsky and Emerson (2015), which compartmentalizes the upper ocean (0-150 m) into a
124 mixed layer box (with variable height) with one meter boxes below. This model assumes that
125 horizontal processes are not important. Because horizontal gradients of oxygen are small, lateral
126 transport has much less influence on this property than fluxes from air-sea gas exchange, vertical
127 advection, and diapycnal eddy diffusion. A detailed assessment of this assumption is given in

Yang et al. (2017). Furthermore, the temperature time series measured by the SOS-Argo (Figure S1) shows no significant intrusions of fronts/eddies, and the continuity of water mass during the study period also allows us to use this simplified model that ignores horizontal processes.

We define ANCP as the flux of organic carbon that escapes the "upper ocean" after a complete seasonal cycle. To be consistent with this definition NCP is integrated vertically from the surface ocean to the winter mixed layer depth, which in this location is roughly equal to the pycnocline depth. Because internal waves cause a 10 to 20 meter variation in the depth of density surfaces in this location, we used the annual mean pycnocline depth as the base of the modeled "upper ocean" to conserve mass in the model. Fluxes across the base of the upper ocean are calculated using measured gradients in oxygen at the density of the pycnocline, independent of its depth.

Oxygen concentration changes over time in the modeled "upper ocean" with depth of h ($dh[O_2]/dt$) are the sum of: gas exchange fluxes ($F_{A\text{-}W}$), vertical advection flux (F_V), diapycnal eddy diffusion (F_{Kz}), entrainment between the mixed layer and the water below (F_E), and net biological oxygen production (J_{NCP}).

$$\frac{dh[O_2]}{dt} = F_{A-W} + F_V + F_{Kz} + F_E + J_{NCP} \quad (1)$$

$F_{A\text{-}W}$ is calculated only for the mixed layer box, using a gas exchange model that includes both diffusion and bubble processes (Emerson and Bushinsky, 2016; Liang et al., 2013). With the time step (3 h) used in our case, the mixed layer change between time steps is always smaller or equal to 1 m, so entrainment occurs only between the mixed layer box and the box below. The entrainment flux (F_E) that gets out of the mixed layer box ends up going into the box below and vice versa, so F_E for these two boxes have the same value but different signs and cancel each

other out. F_V is calculated from Ekman pumping rate (derived from wind speed) and oxygen gradient from SOS-Argo measurements. F_{Kz} is calculated with oxygen gradient and diapycnal eddy diffusion coefficient from Cronin et al. (2015), which decreases with depth from the base of the mixed layer to a background value of 10^{-5} m^{-2} s^{-1} (Whalen et al., 2012) with a 1/e scaling described in Sun et al. (2013) (See also Bushinsky and Emerson, 2015). For the mixed layer reservoir F_{kz} and F_V are considered only at the base of the box. For all the boxes below the mixed layer, F_{kz} and F_V are considered both on the top and at the base of each box. Biological oxygen production, J_{NCP}, is the difference between the calculated fluxes and the measured time rate of change (left hand side of Equation 1). This value is converted from oxygen to carbon production (i.e. ANCP) using a constant oxygen to carbon ratio of 1.45 (Hedges et al., 2002).

The uncertainty of ANCP was estimated using a Monte Carlo approach. Confidence intervals for oxygen measurements and the gas exchange mass transfer coefficients used in the oxygen mass balance model were assigned to the model, and varied randomly while ANCP was calculated in two hundred runs for each calculation. Details of this approach are presented in the supporting information and Yang et al. (2017).

2.2.2 DIC mass balance model

We used a similar mass balance model for DIC, in which the base of the modeled "upper ocean" is set to the annual mean pycnocline depth (the same as the oxygen mass balance model). This choice of the upper ocean depth distinguishes this model from the mixed layer model used in Fassbender et al. (2016). Fluxes at the base of the upper ocean in our model use DIC gradients, diapycnal eddy diffusion coefficients, and upwelling velocities determined at the mean pycnocline depth while Fassbender et al. (2016) used the values at the bottom of the mixed layer. Because the OSP surface mooring provided only the mixed layer DIC data, we assumed that

there is no annual net DIC change in the depth region between the mixed layer and the annual mean pycnocline depth. The depth gradient of DIC used to calculate fluxes across the pycnocline was calculated from measured oxygen gradients assuming dO_2/dz to dDIC/dz ratio of 1.45 (Hedges et al., 2002). Thus, we assume for this calculation that the DIC change at the pycnocline depth is only due to degradation of organic matter, which ignores the change due to $CaCO_3$ dissolution (Fassbender et al., 2016). For the DIC mass balance the multi-layer model is equivalent to a one-layer model:

$$\frac{\mathrm{dh[DIC]}}{\mathrm{dt}} = \mathrm{F_{A-W}} + \mathrm{F_V} + \mathrm{F_{Kz}} + \mathrm{F_E} + \mathrm{J_{NCP}} \quad (2)$$

where the DIC change (dh[DIC]/dt) for the modeled upper ocean (the air-sea interface to the mean depth of the pycnocline) is due to air-water CO_2 exchange ($F_{A\text{-}W}$) at the air-sea interface, vertical advection (F_V) and diapycnal eddy diffusion (F_{Kz}) at the base of the modeled "upper ocean", and net biological carbon production (J_{NCP}) in between. For this one-layer model, entrainment occurred within the same layer (box) and therefore there is no net entrainment flux ($F_E = 0$). The air-sea gas-exchange mass transfer coefficient is calculated as a function of wind speed using equations from Wanninkhof (2014). The DIC gradients used for F_V and F_{Kz} are derived from oxygen gradients at the pycnocline depth as described above.

2.3 Temperature dependence of NCP derived from the metabolic theory of ecology

The correlation between NCP variation and environmental temperature could be attributed to the temperature dependence of planktonic metabolism. Regaudie-De-Gioux and Duarte (2012) derived the temperature dependences of gross primary production (GPP) and community respiration (CR) using the metabolic theory of ecology and a large historical dataset on volumetric planktonic metabolism in different seasons and ocean regimes (1156 estimates of

volumetric metabolic rates and the corresponding water temperature). Equations 3 & 4below are their linear regressions between the natural logarithm of the specific metabolic rates (*GPP/Chla* and *CR/Chla*) and the inverted water temperature (*1/kT*),

$$Ln\frac{GPP}{Chla} = a_p\frac{1}{kT} + b_p \quad (3)$$

$$Ln\frac{CR}{Chla} = a_r\frac{1}{kT} + b_r \quad (4)$$

where *Chla* is the chlorophyll-*a* concentration, *k* is the Boltzmann's constant, *T* is the environmental temperature in Kelvin, and a_p, b_p, a_r, b_r are slopes and intercepts for each linear regression. The temperature dependence of *GPP/CR* can be derived by combining Equations 3 & 4:

$$\frac{GPP}{CR} = EXP\left[(a_p - a_r)\frac{1}{kT} + (b_p - b_r)\right] \quad (5)$$

Since the community respiration (CR) includes the respiration of both autotrophs and heterotrophs, NCP can be calculated as the difference between GPP and CR.

$$NCP = GPP - CR = GPP\left(1 - \frac{1}{\frac{GPP}{CR}}\right) \quad (6)$$

Combining Equations 5 and 6 gives us the NCP-temperature relationship.

$$NCP = GPP\left\{1 - \frac{1}{EXP[(a_p - a_r)\frac{1}{kT} + (b_p - b_r)]}\right\} \quad (7)$$

3 Results

3.1 Oxygen and DIC measurements

The evolutions of density, oxygen concentration, and the oxygen anomaly in percent supersaturation ($\Delta O_2 = ([O_2]/[O_2]_{sat} - 1) \times 100$) determined by the profiling float at OSP from 2012 to 2016 are presented in Figure 4(a-c). The saturation concentration of oxygen ($[O_2]_{sat}$) was calculated using equations from Garcia and Gordon (1992, 1993). The thin black line indicates the mixed layer depth, which is defined by a density offset from the value at 10 m using a threshold of 0.03 kg m^{-3} (de Boyer Montégut, 2004). The thick blue line indicates the pycnocline with a density of σ_θ = 25.8 kg m^{-3}, which follows $[O_2]$ gradients well (Figure 4b). The white boxes indicate the modeled "upper ocean" for each year, in which base of the modeled "upper ocean" is the mean pycnocline depth for each year. Oxygen in the mixed layer was supersaturated from mid April to October/November, and near saturation or slightly undersaturated for the rest of the year (Figure 4c).

The evolution of salinity normalized DIC in the mixed layer determined by the OSP mooring is presented in Figure 4d. The pCO_2 sensor stopped working during two periods in 2013 and 2016 (indicated with dash line boxes), and therefore the data for these two periods is filled with interpolated values. Strong summertime DIC drawdown was observed in each year with the lowest DIC around September.

3.2 Annual Net Community Production

All the terms of the oxygen mass balance calculation in each year are presented in Table 2a. The ANCP results (2.4 ± 0.6, 0.8 ± 0.4, 2.1 ± 0.4 and 1.6 ± 0.4 mol C m^{-2} yr^{-1}, with a mean value of 1.7 ± 0.7 mol C m^{-2} yr^{-1}) indicate that ANCP initially decreased after warmer water invaded this area (2013-14) and then returned to the "pre-blob" value of 2012-13 in subsequent years. Given the uncertainty in the estimate of ANCP in each year, the value during year 2013-14 is significantly different at the 95% confidence interval (as determined by t-test, Bethea et al.,

1975). With the exception of the unusually low value for 2013-14, ANCP values from oxygen mass balance calculation are very close to the historical ANCP estimates at OSP (2.3 ± 0.6 mol C m^{-2} yr^{-1}, Emerson 2014).

If we integrate the ANCP from the ocean surface to the depth of the mixed layer ($ANCP_{mixed\ layer}$ in Table 2a) instead of to the annual mean depth of the pycnocline, the results are higher (3.4, 1.3, 2.3 and 2.3 mol C m^{-2} yr^{-1}, with a mean value of 2.4 ± 0.9 mol C m^{-2} yr^{-1}). While the mean value is higher because it includes some organic carbon flux that is degraded between the mixed layer and pycnocline in summer, the annual trend, in which ANCP is significantly lower in year two (2013-14), is the same as that in which ANCP values were determined for the depth interval above the pycnocline.

In comparison, ANCP values determined from DIC mass balance are 2.0, 2.1, 2.6, 3.0 mol C m^{-2} yr^{-1}, with a mean value of 2.4 ± 0.5 mol C m^{-2} yr^{-1} (Table 2b). The mean value is similar within the errors of the value determined from the oxygen mass balance (1.7 ± 0.7 mol C m^{-2} yr^{-1}) but there is no significant change between the second year (2013-14) and those before and after. The somewhat higher value could be due to the assumption we made about DIC change below the mixed layer or because we neglected horizontal advection (See Discussion).

3.3 Phytoplankton abundance and community composition

Chl-*a* concentration, an indicator of phytoplankton biomass, was about 50% lower (0.22 mg m^{-3}) during the period from August 2013 to June 2014 than during the rest of the 2012 to 2016 period (Figure 5a) and the historical annual average at OSP (Peña and Varela, 2007). Chl-*a* resumed to the 2012-13 level in August 2014 and had a significant increase in the summer of 2016. 19'-hexanoyloxyfucoxanthin (Hex), which is mainly derived from prymnesiophytes, was found to be the most abundant pigment after T-chla (Figure 5b). Fucoxanthin (Fuco), a pigment

associated with diatoms, haptophytes and pelagophytes, was also abundant and showed increased concentration (0.54 mg m^{-3}) in June 2016, coinciding with increased T-chla. After Hex, and Fuco, chlorophyll-b was the most abundant pigment (0.36 to 0.27 mg m^{-3}), indicating the presence of green algae. We also detected occasionally lutein (0-0.125 mg m^{-3}), violaxanthin (0-0.012 mg m^{-3}) and, prasinoxanthin (0-0.005 mg m^{-3}), which are biomarkers for green algae.

The CHEMTAX analysis detected the presence of seven classes of phytoplankton (Figure 5c) and showed an increase in the relative contribution of cyanobacteria and chlorophytes during the "Blob" period with the highest proportion of the former group in June of 2014 and the latter in June 2015 (Figure 5c). There was also a decrease in the abundance of diatoms from August 2013 to June 2015. The remainder of the phytoplankton community was primarily composed of haptophytes and the contribution of the other phytoplankton groups was variable and showed no consistent year-to-year variability. By August 2015 the phytoplankton community had returned to a similar relative composition as observed in 2012-13, with nanoplankton (mostly haptophytes) being dominant and with microplankton (diatoms and dinoflagellates) increasing in abundance. The input matrix (Table 1a) appeared to describe the environment well since the final pigment ratio matrix did not differ dramatically from the initial input values.

4 Discussion

4.1 Comparisons of ANCP from oxygen and DIC mass balances

Although the ANCP are integrated to the same depth in our oxygen and DIC mass balance models, as mentioned in Section 3.2, the ANCP determined from DIC mass balance (4-year mean: 2.4 ± 0.5 mol C m^{-2} yr^{-1}) is somewhat higher than the value determined from oxygen mass balance (4-year mean: 1.7 ± 0.7 mol C m^{-2} yr^{-1}), but still within the error of the model.

There are two possible reasons for such discrepancy. First of all, due to the lack of DIC data below the mixed layer, for the DIC model we made an assumption that there is no annual net DIC change in the depth region between the mixed layer and the annual mean pycnocline depth. With this assumption, the ANCP from DIC mass balance is higher because it includes the organic carbon that is degraded between the mixed layer and pycnocline in summer, so the ANCP from DIC mass balance (4-year mean: 2.4 ± 0.5 mol C m^{-2} yr^{-1}) is very similar to the mixed layer ANCP determined from our oxygen mass balance model (4-year mean: 2.4 ± 0.9 mol C m^{-2} yr^{-1}) and the mixed layer ANCP determined by Fassbender et al. (2016) (2 ± 1 mol C m^{-2} yr^{-1}). The second possible reason that the 4-year mean value of ANCP determined from the DIC mass balance is higher than the value determined from the oxygen mass balance is horizontal advection. Because gas exchange resets the oxygen saturation anomaly for oxygen about ten times faster than CO_2, the DIC mass balance is more vulnerable to horizontal fluxes than the O_2 mass balance. If we assumed that the difference in ANCP estimated from these two tracers (0.7 mol C m^{-2} yr^{-1}) is due to horizontal advection, and calculate the horizontal DIC gradient using the 4-year mean horizontal velocity at OSP of 0.08 m s^{-1}, we found that a horizontal DIC gradient of 1×10^{-8} mol m^{-4} is required to cause the difference of 0.7 mol C m^{-2} yr^{-1}, which is possible at this location (horizontal DIC gradient along the 4-year mean horizontal flow at OSP is about $2\sim3\times10^{-8}$ mol m^{-4} from GLODAP v1.1 gridded product, Key et al., 2004).

As for the inter-annual changes in ANCP, the oxygen mass balance calculation shows that ANCP had a significant decrease in 2013-14 and then returned to the "pre-blob" level in the following years whereas ANCP calculated from DIC mass balance does not show this trend. Since air-sea exchange is a large part of the flux mass balance for both oxygen and CO_2 (Table 2), a likely reason for this discrepancy is due to the shorter residence time with respect to gas

exchange for the oxygen compared to the CO_2 saturation anomalies. An example of the residence time calculation is included in the supporting information where it indicates that the gas exchange residence time in the upper ocean for oxygen is about one month and that for CO_2 is about one year (See also Emerson and Hedges, 2008, Chapter 11). Thus, the biologically induced saturation anomaly for oxygen responds fast enough to record annual changes whereas that for pCO_2 and DIC does not. On the other hand, as discussed above, since DIC mass balance is more vulnerable to horizontal flux than oxygen mass balance, the DIC signal might already been "smoothed" by the horizontal flux, which may also explain why the inter-annual ANCP changes were not observed by using the DIC mass balance approach. Alternatively, the production ratio of particulate organic carbon (POC) and particulate inorganic carbon (PIC) may cause the inter-annual variation of DIC mass balance. However, in our case since there was no significant bloom of haptophytes (e.g. coccolithophore) during the study period (Figure 5c), it is unlikely that the inter-annual change in POC/PIC ratio would affect the ANCP result calculated from DIC mass balance. Hence, from this point forward we will focus on analyzing the factors that might influence ANCP variations determined by the oxygen mass balance model.

4.2 Causes of ANCP decrease

In the following paragraphs, we analyze connections between ANCP decrease and the "Blob" temperature anomaly in the context of multiple physical and biological processes, including the choices of start time from which ANCP are calculated, the base depth of the modeled "upper ocean", planktonic metabolism, and changes in phytoplankton community composition.

Our observations began in June 2012, 10 – 12 months before the positive SST anomalies. To determine whether the start date for determining the ANCP values affects the results, we

began the time series on four different months (Table 3). We are somewhat limited because there is only about 12 "pre-blob" months before June 2012. However, as shown in Table 3, as long as there are more "pre-blob" months than "Blob-affected" months in the 1st year, the significant ANCP decrease from 1st to 2nd year is still observed and the trend of ANCP variation for those 4 years remains.

To determine whether the annual mean pycnocline depth (the white rectangles in Figure 4a-4c) influences the ANCP trends we calculated ANCP using the 4-year mean depth of 100 m for the modeled "upper ocean". The ANCP results only change slightly (2.6, 1.0, 1.9, and 1.6 mol C m^{-2} yr^{-1}) and the decrease in 2013-14 is still statistically significant, indicating that the different base depth used for the modeled "upper ocean" is not the key factor that causes ANCP changes.

To test if the temperature dependence of planktonic metabolism is strong enough to cause the ANCP decline we observed (e.g. 1.6 mol C m^{-2} yr^{-1} between 2012-13 and 2013-14), we calculated the GPP from measured NCP of year 1 (2012-13) using Equation 7, and assumed GPP was constant for all four years so we could then determine the effect of temperature on NCP based on the metabolic theory of ecology (Equation 7). Since the specific phytoplankton growth rate increases with increasing temperature (e.g. Regaudie-De-Gioux and Duarte, 2012; Chen and Laws, 2017), if phytoplankton biomass would have remained the same during the "blob", GPP would have increased. Thus, assuming a constant GPP in this calculation is somewhat speculative, but it at least provides a first-order assessment of the metabolic temperature effect on ANCP. The parameterizations derived with datasets from the Arctic were used (Regaudie-De-Gioux and Duarte, 2012), because it gives the largest change in ANCP. The results (Table 4) indicate that temperature dependence of planktonic metabolism is not strong enough to account

for the measured ANCP decrease in the 2nd year (2013-14), suggesting that this is not the major reason for the observed ANCP decline.

Having ruled out the above likely candidates, we suggest that the observed ANCP decrease is most likely linked to the changes in GPP (e.g. low phytoplankton biomass observed in the 2nd year Figure 5a) and phytoplankton community composition (Figure 5c). In general, larger phytoplankton (i.e. microplankton) are more efficient exporters than smaller nanoplankton and picoplankton (e.g., Chen and Laws, 2016). Given the lower export rates of picoplankton (e.g. cyanobacteria) than those of larger phytoplankton (e.g. diatoms) the observed changes in phytoplankton community composition (Figure 5b) in 2013-14, which included a decrease in the relative abundance of diatoms, and an increase in the relative abundance of cyanobacteria and green algae (chlorophytes), could have further contributed to the decrease in ANCP. After the initial response to the temperature anomaly, chl-*a* concentration and the phytoplankton community composition returned to a level similar to those observed before the warming occurred, suggesting that the plankton community rapidly adapted to the higher temperature and prevailing environmental conditions. These changes in GPP and phytoplankton community composition could be ultimately in response to the lack of micronutrients like iron (due to enhanced stratification from the "blob" that restricted the vertical supply), which has been shown to regulate phytoplankton biomass and composition in this high-nutrient, low-chlorophyll region (e.g. Hamme et al., 2010; Marchetti et al., 2006). Unfortunately, we do not have iron data available to confirm that at this time.

5 Conclusions

The annual net community production (ANCP) at Ocean Station Papa (OSP) in the subarctic Northeast Pacific Ocean was determined from June 2012 to June 2016 to examine the

371 effect of the temperature anomaly on the efficiency of carbon export. The ANCP determined by
372 oxygen mass balance had a four year mean value of 1.7 ± 0.7 mol C m^{-2} yr^{-1}, whereas ANCP
373 determined by DIC mass balance gives a somewhat higher mean value (2.4 ± 0.5 mol C m^{-2} yr^{-1}).
374 ANCP for individual years determined from O_2 mass balance showed a significant decrease in
375 year 2 (2013-14) after the onset of the temperature anomaly, but no significant decrease in
376 ANCP was found when calculated with DIC mass balance. We believe that this indicates that the
377 DIC concentration and pCO_2 respond too slowly to capture annual changes in ANCP. Based on
378 our observations and historical ANCP estimates at OSP as reference, we found there was a
379 significant ANCP decrease in 2013-14 due to the warm anomaly, which is consistent with the
380 findings from concurrent phytoplankton data. Possible mechanisms for the observed decrease in
381 ANCP by the oxygen mass balance in the second year were analyzed in the context of multiple
382 physical and biological processes that could be affected by temperature anomaly. Our analysis
383 showed that the ANCP decrease, as well as changes in phytoplankton abundance and community
384 composition, was most likely due to changes in GPP after the "Blob" entered the area. These
385 changes could be ultimately in response to the lack of micronutrients like iron during the "Blob"
386 period. However, the ultimate cause cannot be specified by our analysis at this time.
387
388 ***Data availability.***
389 Float data are available online (https://sites.google.com/a/uw.edu/sosargo/home). Mooring data
390 is available online at: http://cdiac.ornl.gov/oceans/Moorings/Papa_145W_50N.html.
391 ***Author contributions.***

BY and SRE designed the experiments. BY developed the model code and process the data. AP provided the data, analysis and interpretation of phytoplankton. BY and SRE prepared the manuscript with contributions from all co-authors.

Competing interests.

The authors declare that they have no conflict of interest.

Acknowledgements.

We thank Dr. Stephen Riser and Dana Swift for their assistance in development of the SOS-Argo float, and scientists of NOAA PMEL and the Institute of Ocean Sciences (IOS) and crews of CCGS John P. Tully, for their work on OSP mooring and Line P cruises. Special thanks are given to Dr. John Crusius for the constructive discussions and comments on this study. This work was supported by National Science Foundation grant OCE-1458888.

References

Allen, A. P., Gillooly, J. F. and Brown, J. H.: Linking the global carbon cycle to individual metabolism, Funct. Ecol., 19(2), 202–213, doi:10.1111/j.1365-2435.2005.00952.x, 2005.

Bethea, R. M., Duran, B. S. and Boullion, T. L.: Statistical methods for engineers and scientists, Marcel Dekker, Inc., New York., 1975.

Bond, N. A., Cronin, M. F., Freeland, H. and Mantua, N.: Causes and impacts of the 2014 warm anomaly in the NE Pacific, Geophys. Res. Lett., 42(9), 3414–3420, doi:10.1002/2015GL063306, 2015.

de Boyer Montégut, C.: Mixed layer depth over the global ocean: An examination of profile data and a profile-based climatology, J. Geophys. Res., 109(C12), C12003, doi:10.1029/2004JC002378, 2004.

Brown, J. H., Gillooly, J. F., Allen, A. P., Savage, V. M. and West, G. B.: TOWARD A METABOLIC THEORY OF ECOLOGY, Ecology, 85(7), 1771–1789, doi:10.1890/03-9000, 2004.

Bushinsky, S. M. and Emerson, S.: Marine biological production from in situ oxygen measurements on a profiling float in the subarctic Pacific Ocean, Global Biogeochem. Cycles, 29(12), 2050–2060, 2015.

Bushinsky, S. M., Emerson, S. R., Riser, S. C. and Swift, D. D.: Accurate oxygen measurements on modified Argo floats using in situ air calibrations, Limnol. Oceanogr. Methods, 2016.

Cavole, L., Demko, A., Diner, R., Giddings, A., Koester, I., Pagniello, C., Paulsen, M.-L., Ramirez-Valdez, A., Schwenck, S., Yen, N., Zill, M. and Franks, P.: Biological Impacts of the 2013–2015 Warm-Water Anomaly in the Northeast Pacific: Winners, Losers, and the Future, Oceanography, 29(2), 273–285, doi:10.5670/oceanog.2016.32, 2016.

Charette, M. A., Bradley Moran, S. and Bishop, J. K. B.: as a tracer of particulate organic carbon export in the subarctic northeast Pacific Ocean, Deep Sea Res. Part II Top. Stud. Oceanogr., 46(11–12), 2833–2861, doi:10.1016/S0967-0645(99)00085-5, 1999.
Chen, B. and Laws, E. A.: Is there a difference of temperature sensitivity between marine phytoplankton and heterotrophs?, Limnol. Oceanogr., doi:10.1002/lno.10462, 2016.
Cronin, M. F., Pelland, N. A., Emerson, S. R. and Crawford, W. R.: Estimating diffusivity from the mixed layer heat and salt balances in the North Pacific, J. Geophys. Res. Ocean., 120(11), 7346–7362, 2015.
Dickson, A. G., Wesolowski, D. J., Palmer, D. A. and Mesmer, R. E.: Dissociation constant of bisulfate ion in aqueous sodium chloride solutions to 250. degree. C, J. Phys. Chem., 94(20), 7978–7985, 1990.
Emerson, S.: Seasonal oxygen cycles and biological new production in surface waters of the subarctic Pacific Ocean, J. Geophys. Res. Ocean., 92(C6), 6535–6544, 1987.
Emerson, S. and Bushinsky, S.: The role of bubbles during air-sea gas exchange, J. Geophys. Res. Ocean., 2016.
Emerson, S. and Hedges, J.: Chemical oceanography and the marine carbon cycle., 2008.
Emerson, S. and Stump, C.: Net biological oxygen production in the ocean—II: Remote in situ measurements of O 2 and N 2 in subarctic pacific surface waters, Deep Sea Res. Part I Oceanogr. Res. Pap., 57(10), 1255–1265, 2010.
Emerson, S., Quay, P., Stump, C., Wilbur, D. and Knox, M.: O2, Ar, N2, and 222Rn in surface waters of the subarctic Ocean: Net biological O2 production, Global Biogeochem. Cycles, 5(1), 49–69, doi:10.1029/90GB02656, 1991.
Emerson, S., Quay, P. and Wheeler, P. A.: Biological productivity determined from oxygen mass balance and incubation experiments, Deep Sea Res. Part I Oceanogr. Res. Pap., 40(11), 2351–2358, 1993.
Emerson, S., Sabine, C., Cronin, M. F., Feely, R., Cullison Gray, S. E. and DeGrandpre, M.: Quantifying the flux of CaCO 3 and organic carbon from the surface ocean using in situ measurements of O 2 , N 2 , pCO 2 , and pH, Global Biogeochem. Cycles, 25(3), n/a-n/a, doi:10.1029/2010GB003924, 2011.
Fassbender, A. J., Sabine, C. L. and Cronin, M. F.: Net community production and calcification from 7 years of NOAA Station Papa Mooring measurements, Global Biogeochem. Cycles, 30(2), 250–267, doi:10.1002/2015GB005205, 2016.
Freeland, H.: A short history of Ocean Station Papa and Line P, Prog. Oceanogr., 75(2), 120–125, doi:10.1016/j.pocean.2007.08.005, 2007.
Freeland, H. J. and Cummins, P. F.: Argo: A new tool for environmental monitoring and assessment of the world's oceans, an example from the N.E. Pacific, Prog. Oceanogr., 64(1), 31–44, doi:10.1016/j.pocean.2004.11.002, 2005.
Garcia, H. E. and Gordon, L. I.: Oxygen solubility in seawater: Better fitting equations, Limnol. Oceanogr., 37(6), 1307–1312, doi:10.4319/lo.1992.37.6.1307, 1992.
Garcia, H. E. and Gordon, L. I.: Erratum: Oxygen Solubility in Seawater: Better Fitting Equations, Limnol. Ocean., 38(3), 656 [online] Available from: http://www.jstor.org/stable/2838040?seq=1, 1993.
Giesbrecht, K. E., Hamme, R. C. and Emerson, S. R.: Biological productivity along Line P in the subarctic northeast Pacific: In situ versus incubation-based methods, Global Biogeochem. Cycles, 26(3), doi:10.1029/2012GB004349, 2012.
Gillooly, J. F., Brown, J. H. and West, G. B.: Effects of Size and Temperature on Metabolic

Rate, Science (80-.)., 293(September), 2248–2252, doi:10.1126/science.1061967, 2001.
Hamme, R. C., Webley, P. W., Crawford, W. R., Whitney, F. A., Degrandpre, M. D., Emerson, S. R., Eriksen, C. C., Giesbrecht, K. E., Gower, J. F. R., Kavanaugh, M. T., Pea, M. A., Sabine, C. L., Batten, S. D., Coogan, L. A., Grundle, D. S. and Lockwood, D.: Volcanic ash fuels anomalous plankton bloom in subarctic northeast Pacific, Geophys. Res. Lett., 37(19), doi:10.1029/2010GL044629, 2010.
Hedges, J. I., Baldock, J. A., G??linas, Y., Lee, C., Peterson, M. L. and Wakeham, S. G.: The biochemical and elemental compositions of marine plankton: A NMR perspective, Mar. Chem., 78(1), 47–63, doi:10.1016/S0304-4203(02)00009-9, 2002.
van Heuven, S., Pierrot, D., Rae, J. W. B., Lewis, E. and Wallace., D. W. R.: MATLAB Program Developed for CO2 System Calculations. ORNL/CDIAC-105b., , doi:10.3334/CDIAC/otg.CO2SYS_MATLAB_v1.1, 2011.
Johnson, K. S., Berelson, W. M., Boss, E. S., Claustre, H., Emerson, S. R., Gruber, N., Körtzinger, A., Perry, M. J. and Riser, S. C.: Observing Biogeochemical Cycles at Global Scales with Profiling Floats and Gliders: Prospects for a Global Array, Oceanography, 22 [online] Available from: http://dx.doi.org/10.5670/oceanog.2009.81, 2009.
Juranek, L. W., Quay, P. D., Feely, R. A., Lockwood, D., Karl, D. M. and Church, M. J.: Biological production in the NE Pacific and its influence on air-sea CO2 flux: Evidence from dissolved oxygen isotopes and O2/Ar, J. Geophys. Res. Ocean., 117(C5), n/a-n/a, doi:10.1029/2011jc007450, 2012.
Key, R. M., Kozyr, A., Sabine, C. L., Lee, K., Wanninkhof, R., Bullister, J. L., Feely, R. A., Millero, F. J., Mordy, C. and Peng, T. H.: A global ocean carbon climatology: Results from Global Data Analysis Project (GLODAP), Global Biogeochem. Cycles, 18(4), 1–23, doi:10.1029/2004GB002247, 2004.
Lee, K., Kim, T.-W., Byrne, R. H., Millero, F. J., Feely, R. A. and Liu, Y.-M.: The universal ratio of boron to chlorinity for the North Pacific and North Atlantic oceans, Geochim. Cosmochim. Acta, 74(6), 1801–1811, 2010.
Liang, J. H., Deutsch, C., McWilliams, J. C., Baschek, B., Sullivan, P. P. and Chiba, D.: Parameterizing bubble-mediated air-sea gas exchange and its effect on ocean ventilation, Global Biogeochem. Cycles, 27(3), 894–905, doi:10.1002/gbc.20080, 2013.
López-Urrutia, A., San Martin, E., Harris, R. P. and Irigoien, X.: Scaling the metabolic balance of the oceans., Proc. Natl. Acad. Sci. U. S. A., 103(23), 8739–44, doi:10.1073/pnas.0601137103, 2006.
Di Lorenzo, E. and Mantua, N.: Multi-year persistence of the 2014/15 North Pacific marine heatwave, Nat. Clim. Chang., (July), 1–7, doi:10.1038/nclimate3082, 2016.
Lueker, T. J., Dickson, A. G. and Keeling, C. D.: Ocean pCO 2 calculated from dissolved inorganic carbon, alkalinity, and equations for K 1 and K 2: validation based on laboratory measurements of CO 2 in gas and seawater at equilibrium, Mar. Chem., 70(1), 105–119, 2000.
Mackey, M. D., Mackey, D. J., Higgins, H. W. and Wright, S. W.: CHEMTAX - A program for estimating class abundances from chemical markers: Application to HPLC measurements of phytoplankton, Mar. Ecol. Prog. Ser., 144(1–3), 265–283, doi:10.3354/meps144265, 1996.
Marchetti, A., Juneau, P., Whitney, F. A., Wong, C. S. and Harrison, P. J.: Phytoplankton processes during a mesoscale iron enrichment in the NE subarctic Pacific: Part II-Nutrient utilization, Deep. Res. Part II Top. Stud. Oceanogr., 53(20–22), 2114–2130, doi:10.1016/j.dsr2.2006.05.031, 2006.
Peña, M. A. and Varela, D. E.: Seasonal and interannual variability in phytoplankton and nutrient

dynamics along Line P in the NE subarctic Pacific, Prog. Oceanogr., 75(2), 200–222, doi:10.1016/j.pocean.2007.08.009, 2007.
Peña, M. A., Nemcek, N. and Robert, M.: Phytoplankton responses to the 2014–2016 warming anomaly in the northeast subarctic Pacific Ocean, Limnol. Oceanogr., 0(0), doi:10.1002/lno.11056, 2018.
Plant, J. N., Johnson, K. S., Sakamoto, C. M., Jannasch, H. W., Coletti, L. J., Riser, S. C. and Swift, D. D.: Net community production at Ocean Station Papa observed with nitrate and oxygen sensors on profiling floats, Global Biogeochem. Cycles, 30(6), 859–879, doi:10.1002/2015GB005349, 2016.
Regaudie-De-Gioux, A. and Duarte, C. M.: Temperature dependence of planktonic metabolism in the ocean, Global Biogeochem. Cycles, 26(1), doi:10.1029/2010GB003907, 2012.
Rose, J. M. and Caron, D. A.: Does low temperature constrain the growth rates of heterotrophic protists? Evidence and implications for algal blooms in cold waters, Limnol. Oceanogr., 52(2), 886–895, doi:10.4319/lo.2007.52.2.0886, 2007.
Sun, O. M., Jayne, S. R., Polzin, K. L., Rahter, B. A. and St. Laurent, L. C.: Scaling Turbulent Dissipation in the Transition Layer, J. Phys. Oceanogr., 43(11), 2475–2489, doi:10.1175/JPO-D-13-057.1, 2013.
Takahashi, T., Olafsson, J., Goddard, J. G., Chipman, D. W. and Sutherland, S. C.: Seasonal variation of CO 2 and nutrients in the high-latitude surface oceans: A comparative study, Global Biogeochem. Cycles, 7(4), 843–878, doi:10.1029/93GB02263, 1993.
Wanninkhof, R.: Relationship between wind speed and gas exchange over the ocean revisited, Limnol. Oceanogr. Methods, 12(JUN), 351–362, doi:10.4319/lom.2014.12.351, 2014.
Whalen, C. B., Talley, L. D. and MacKinnon, J. A.: Spatial and temporal variability of global ocean mixing inferred from Argo profiles, Geophys. Res. Lett., 39(17), doi:10.1029/2012GL053196, 2012.
Wong, C. ., Waser, N. A. ., Nojiri, Y., Whitney, F. ., Page, J. . and Zeng, J.: Seasonal cycles of nutrients and dissolved inorganic carbon at high and mid latitudes in the North Pacific Ocean during the Skaugran cruises: determination of new production and nutrient uptake ratios, Deep Sea Res. Part II Top. Stud. Oceanogr., 49(24–25), 5317–5338, doi:10.1016/S0967-0645(02)00193-5, 2002a.
Wong, C. S.: Analysis of trends in primary productivity and chlorophyll-a over two decades at Ocean Station P (50°N, 145°W) in the subarctic northeast Pacific Ocean, Can. J. Fish. Aquat. Sci., 121, 107–117 [online] Available from: http://ci.nii.ac.jp/naid/10009665016/en/ (Accessed 4 February 2017), 1995.
Wong, C. S., Waser, N. A. D., Nojiri, Y., Johnson, W. K., Whitney, F. A., Page, J. S. C. and Zeng, J.: Seasonal and Interannual Variability in the Distribution of Surface Nutrients and Dissolved Inorganic Carbon in the Northern North Pacific: Influence of El Ni{ñ}o, J. Oceanogr., 58(2), 227–243, doi:10.1023/A:1015897323653, 2002b.
Yang, B., Emerson, S. R. and Bushinsky, S. M.: Annual net community production in the subtropical Pacific Ocean from in situ oxygen measurements on profiling floats, Global Biogeochem. Cycles, 31(4), doi:10.1002/2016GB005545, 2017.
Zapata, M., F. Rodrigues, and J. L. Garrido. 2000. Separation of chlorophylls and carotenoids from marine phytoplankton: a new HPLC method using a reversed phase C-8 column and pyridine-containing mobile phases. Mar. Ecol. Prog. Ser. **195**: 29–45. doi:10.3354/meps195029.

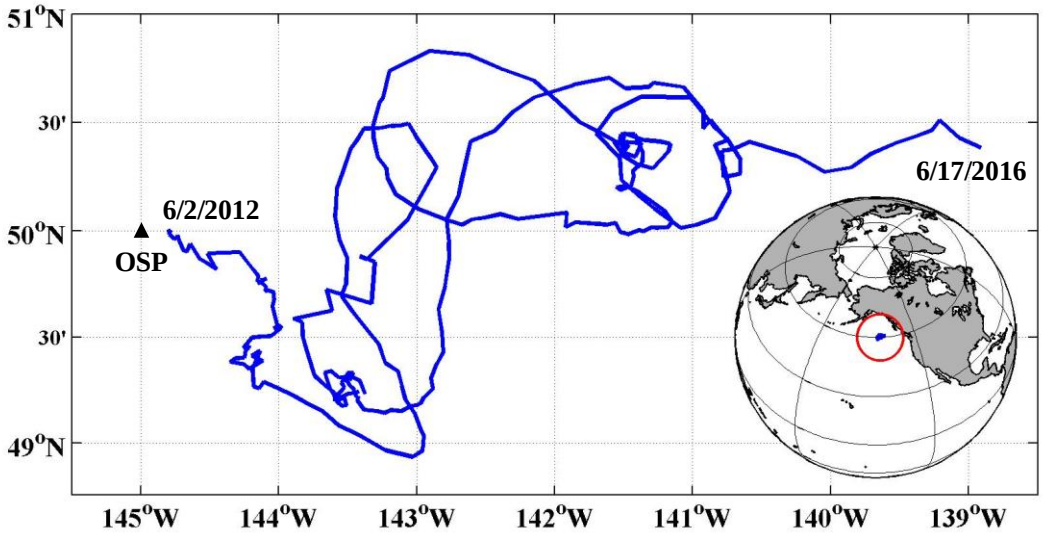

Figure 1 Study area and float path from 2012 to 2016. The black triangle indicates the position of Ocean Station Papa (OSP) Mooring, and the blue line indicates the trajectory of the SOS-Argo float which was within roughly a 2^{o} (N-S) × 6^{o} (E-W) box.

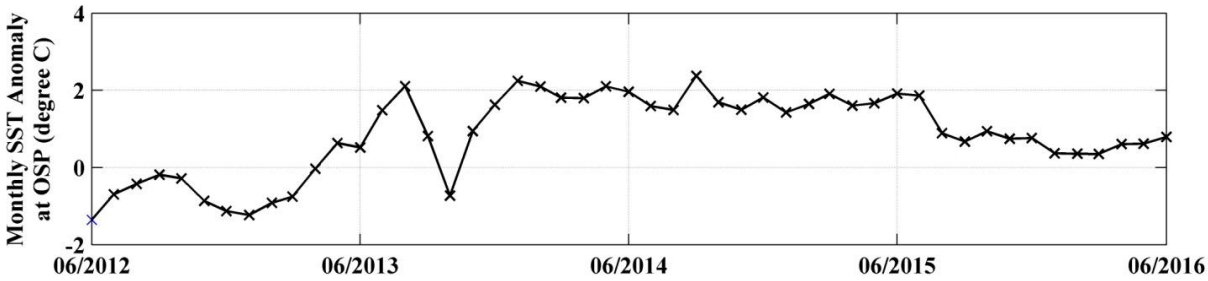

Figure 2 Monthly SST Anomaly at Ocean Station Papa (OSP). The anomaly is defined as the difference between the measured SST and the mean of 1971-2000. Data are from: http://iridl.ldeo.columbia.edu/maproom/Global/Ocean_Temp/Anomaly.html

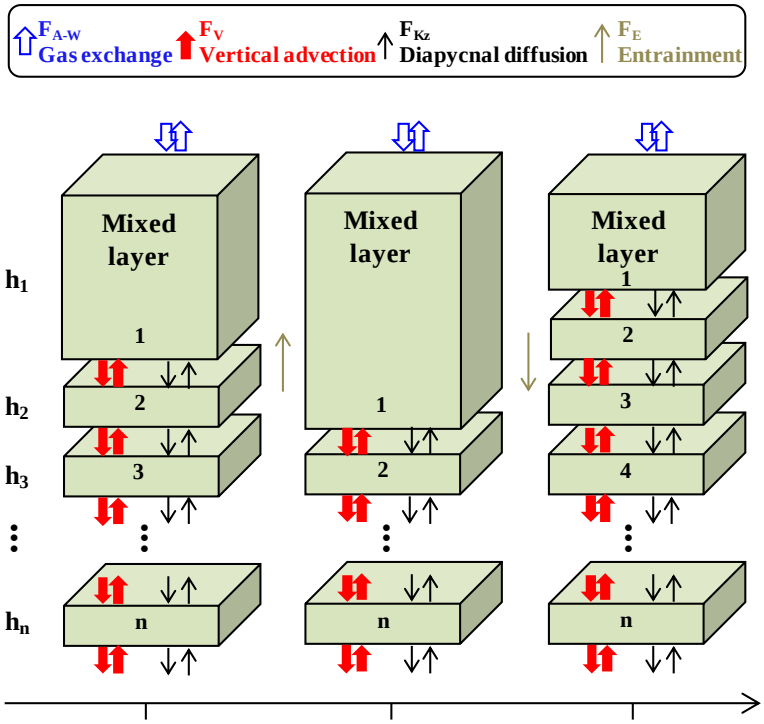

Figure 3 Schematic of the multi-layer upper ocean oxygen mass balance model (adapted from *Bushinsky and Emerson*, 2015). Fluxes (F) are from air-sea gas exchange ($F_{A\text{-}W}$, including diffusion and bubble processes), vertical advection (F_V), diapycnal eddy diffusion (F_{Kz}), and entrainment (F_E).

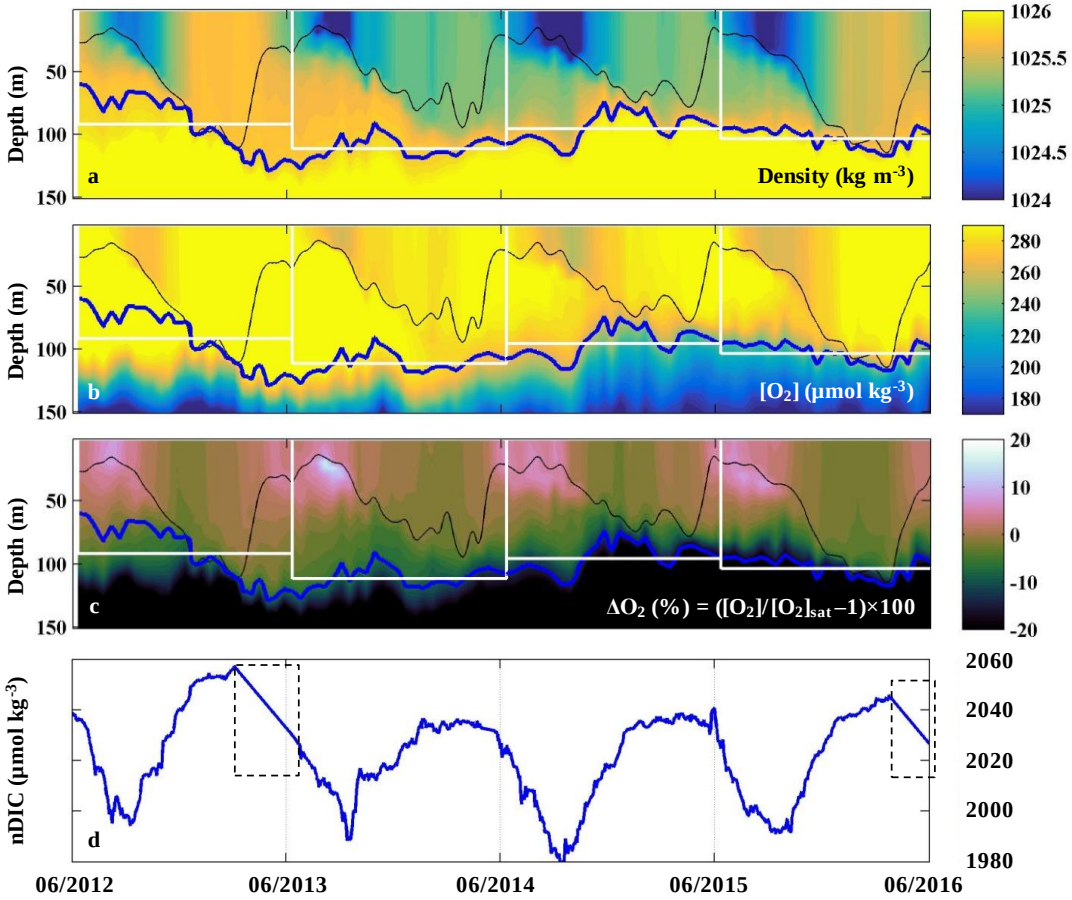

Figure 4 (a-c) Upper ocean density, oxygen concentration, and oxygen supersaturation ΔO_2 (%) from the SOS-Argo float at OSP. The thin black line indicates the mixed layer depth, the thick blue line indicates the pycnocline depth, and the white rectangles indicate the modeled "upper ocean" for each of the four years that ANCP were calculated. (d) Mixed layer DIC normalized to a surface salinity at OSP (S= 32.5) from June 2012 to June 2016. Dash line boxes indicate periods when the pCO2 data were not available and thus were filled with a straight line interpolation.

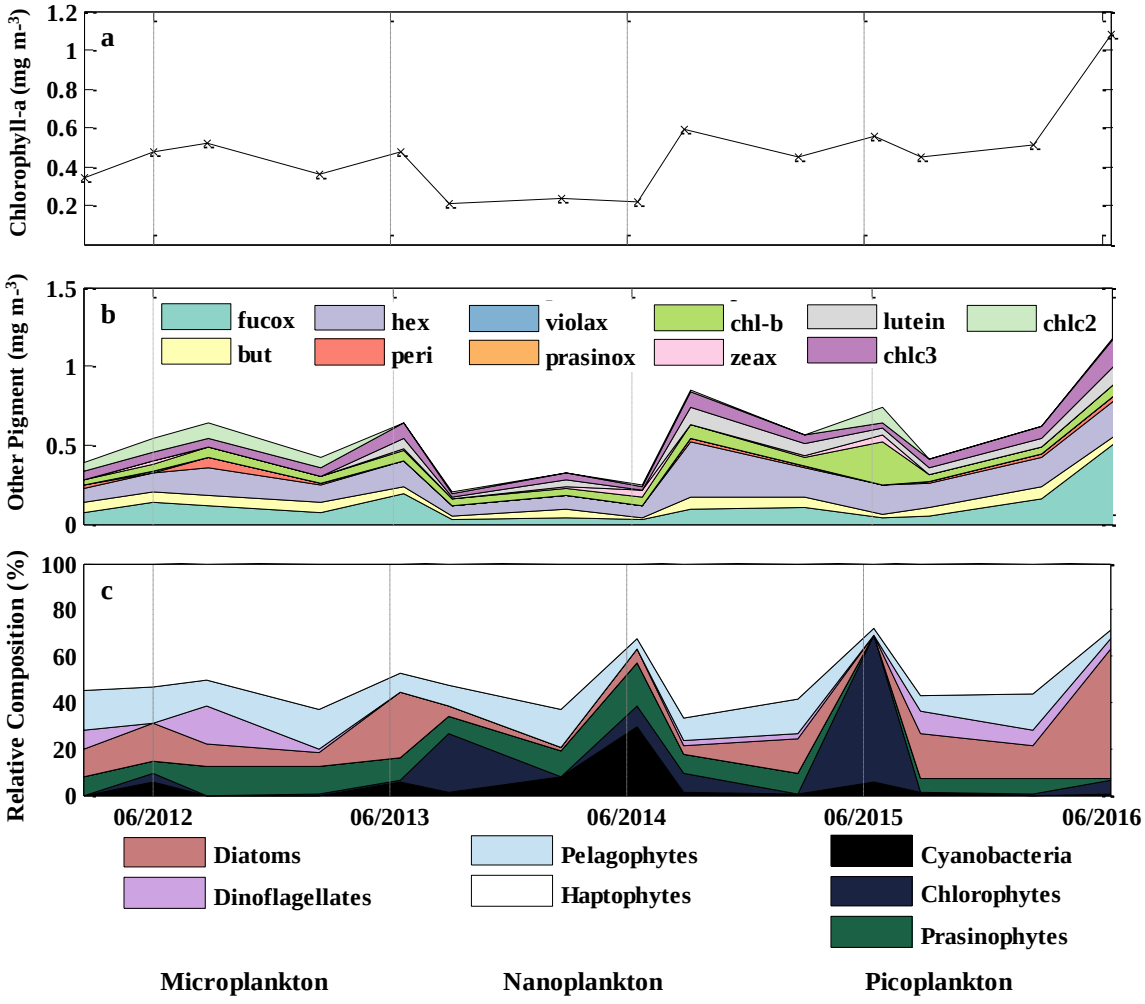

Figure 5 Mixed layer mean (a) chl-*a* concentration (mg m^{-3}), (b) other pigment concentration (mg m^{-3}), and (c) relative phytoplankton composition (%) at OSP. Values were determined from HPLC pigment analysis of samples collected in February, June, and August for each year from 2012 to 2016.

Table 1. Pigment:Chl *a* ratios for eight algal groups: (a) CHEMTAX initial ratio matrix, and (b) ranges of final pigment ratios obtained by CHEMTAX on the pigment data.

	Chl c_3	Chl c_2	Peri	But	Fuco	Pras	Viola	Hex	Allo	Zea	Lut	Chl *b*	Chl *a*
(a)													
Cyano	0	0	0	0	0	0	0	0	0	0.64	0	0	1
Chloro	0	0	0	0	0	0	0.049	0	0	0.032	0.17	0.32	1
Prasino	0	0	0	0	0	0.25	0.054	0	0	0.058	0.021	0.73	1
Crypto	0	0.2	0	0	0	0	0	0	0.38	0	0	0	1
Diatoms	0.08	0.28	0	0	0.99	0	0	0	0	0	0	0	1
Dinofla	0	0.22	0.56	0	0	0	0	0	0	0	0	0	1
Pelago	0.22	0	0	0.64	0.772	0	0	0	0	0	0	0	1
Hapto	0.18	0.21	0	0.039	0.289	0	0	0.47	0	0	0	0	1
(b)													
Cyano	0	0	0	0	0	0	0	0	0	0.48-0.85	0	0	1
Chloro	0	0	0	0	0	0	0.02-0.15	0	0	0.03-0.04	0.06-0.21	0.26-0.45	1
Prasin	0	0	0	0	0	0.04-0.23	0.02-0.06	0	0	0.02-0.06	0.017-0.022	0.72-1.12	1
Crypto	0	0.15-0.23	0	0	0	0	0	0	0.34-0.44	0	0	0	1
Diatoms	0.05-0.09	0.21-0.3	0	0	0.8-1.15	0	0	0	0	0	0	0	1
Dinofla	0	0.19-0.26	0.45-0.64	0	0	0	0	0	0	0	0	0	1
Pelago	0.11-0.25	0	0	0.68-1.15	0.22-0.82	0	0	0	0	0	0	0	1
Hapto	0.05-0.22	0.16-0.26	0	0.037-0.068	0.07-0.25	0	0	0.58-0.81	0	0	0	0	1

Abbreviations: Cyano, cyanobacteria; Chloro, chlorophytes; Prasino, prasinophytes; Crypto, cryptophytes; Dinofla, dinoflagellates; Pelago, pelagophytes; Hapto, haptophytes; Chl c_3, chlorophyll c_3; Chl c_2, chlorophyll c_2; Peri, peridinin; But, 19'-butanoyloxyfucoxanthin; Fuco, fucoxanthin; Pras, prasinoxanthin; Viola, violaxanthin; Hex, 19'-hexanoyloxyfucoxanthin; Allo, alloxanthin; Zea, zeaxanthin; Lut, lutein; Chl *b*, chlorophyll *b*; Chl *a*, chlorophyll.

Table 2 Annual net community production (ANCP) determined from (a) O_2 mass balance, and (b) DIC mass balance. The annually integrated fluxes for each of the important terms (columns 4-9) indicate that the air sea flux and biological production terms dominate for both tracers. Two ANCP values are given in (a): one integrated from the ocean surface to the depth of annual mean pycnocline (column 3), ANCP, and another value integrated over the depth of the mixed layer, $ANCP_{mixed\ layer}$. Only the former is a measure of the biological organic carbon that escapes the upper ocean on an annual basis (see text).

a

Year	**Time Period** (June to June)	**h** (m)	**Annual oxygen mass balance** (mol O_2 m^{-2} yr^{-1}) $dh[O_2]/dt = F_{A\text{-}W} + F_E + F_{Kz} + F_v + J_{NCP}$						**ANCP** = $J_{NCP}/1.45$ (mol C m^{-2} yr^{-1})	**$ANCP_{mixed\ layer}$** (mol C m^{-2} yr^{-1})
			$dh[O_2]/dt$	$F_{a\text{-}w} = F_s + F_b$	F_E	F_{Kz}	F_V	J_{NCP}		
1	2012-13	91	-0.7	-2.9	0	-0.6	-0.6	3.5	2.4 ± 0.6	3.4
2	2013-14	111	-1.3	-1.5	0	-0.8	-0.2	1.2	0.8 ± 0.4	1.3
3	2014-15	95	-0.6	-1.7	0	-0.9	-1.0	3.0	2.1 ± 0.4	2.3
4	2015-16	103	0.8	-0.1	0	-0.7	-0.3	2.3	1.6 ± 0.4	2.3

b

Year	**Time Period** (June to June)	**h** (m)	**Annual DIC mass balance** (mol C m^{-2} yr^{-1}) $dh[DIC]/dt = F_{A\text{-}W} + F_E + F_{Kz} + F_v + J_{NCP}$						**ANCP** = - J_{NCP} (mol C m^{-2} yr^{-1})
			$dh[DIC]/dt$	$F_{a\text{-}w}$	F_E	F_{Kz}	F_V	J_{NCP}	
1	2012-13	91	-0.2	1.0	0	0.7	0.1	-2.0	2.0
2	2013-14	111	-0.1	1.5	0	0.4	0.1	-2.1	2.1
3	2014-15	95	0.05	2.0	0	0.5	0.1	-2.6	2.6
4	2015-16	103	-0.04	2.0	0	0.9	0.1	-3.0	3.0

Table 3 ANCP calculated from O_2 mass balance with different start dates to determine if the chosen annual period affects the conclusions (see text).

Start Time		6/10/12	7/10/12	8/10/12
ANCP (mol C m^{-2} yr^{-1})	1st year (2012-13)	2.4	2.3	2.4
	2nd year (2013-14)	0.8	0.9	0.7
	3rd year (2014-15)	2.1	2.6	2.5
	4th year (2015-16)	1.6	-	-

Table 4 Comparisons of ANCP measured with O_2 mass balance and ANCP predicted from the temperature dependence parameterization of planktonic metabolism using parameters from the Arctic Ocean [*Regaudie-De-Gioux and Duarte*, 2012]. Gross primary production (GPP) is calculated from ANCP in year 1 and Equation 7, and it is assumed to be the same through years 1 – 4. $ANCP_{diff} = 2.4$ (mol C m-2 yr^{-1}) – $ANCP_{Predicted\ or\ Measured}$

Year	**Mean temperature (^oC)**	**ANCP** (mol C m^{-2} yr^{-1})		**$ANCP_{diff}$** (mol C m^{-2} yr^{-1})	
		Predicted	Measured	Predicted	Measured
1	8.4	-	2.4	-	-
2	10.4	1.9	0.8	-0.5	-1.6
3	10.8	1.9	2.1	-0.5	-0.3
4	9.9	2.1	1.6	-0.3	-0.8